



This is a repository copy of *Achieving over 11% power conversion efficiency in PffBT4T-2OD-based ternary polymer solar cells with enhanced open-circuit-voltage and suppressed charge recombination.*

White Rose Research Online URL for this paper:
<http://eprints.whiterose.ac.uk/125585/>

Version: Accepted Version

Article:

Li, W., Cai, J., Cai, F. et al. (6 more authors) (2018) Achieving over 11% power conversion efficiency in PffBT4T-2OD-based ternary polymer solar cells with enhanced open-circuit-voltage and suppressed charge recombination. *Nano Energy*, 44. pp. 155-163. ISSN 2211-2855

<https://doi.org/10.1016/j.nanoen.2017.12.005>

Reuse

This article is distributed under the terms of the Creative Commons Attribution-NonCommercial-NoDerivs (CC BY-NC-ND) licence. This licence only allows you to download this work and share it with others as long as you credit the authors, but you can't change the article in any way or use it commercially. More information and the full terms of the licence here: <https://creativecommons.org/licenses/>

Takedown

If you consider content in White Rose Research Online to be in breach of UK law, please notify us by emailing eprints@whiterose.ac.uk including the URL of the record and the reason for the withdrawal request.



eprints@whiterose.ac.uk
<https://eprints.whiterose.ac.uk/>

Achieving over 11% power conversion efficiency in PffBT4T-2OD-based ternary polymer solar cells with enhanced open-circuit-voltage and suppressed charge recombination

Wei Li^{1,2}, Jinlong Cai^{1,2}, Feilong Cai^{1,2}, Yu Yan^{1,2}, Hunan Yi³, Robert S. Gurney^{1,2}, Dan Liu^{1,2}, Ahmed Iraqi³, Tao Wang^{1,2*}

¹School of Materials Science and Engineering, Wuhan University of Technology, Wuhan 430070, China E-mail: twang@whut.edu.cn

²State Key Laboratory of Silicate Materials for Architectures, Wuhan University of Technology, Wuhan 430070, China

³Department of Chemistry, University of Sheffield, Sheffield S3 7HF, UK

Abstract

Fabricating ternary solar cells (TSCs) is a promising strategy to improve the power conversion efficiency of organic photovoltaics without introducing sophisticated processing procedures. We report in this work high efficiency TSCs with the maximum PCE over 11% by introducing a medium band gap conjugated polymer PCDTBT8 into the PffBT4T-2OD:PC₇₁BM binary photovoltaic system. Morphological investigation shows that the third component PCDTBT8 locates at the interface between PffBT4T-2OD and PC₇₁BM without disrupting the crystallization of PffBT4T-2OD to maintain decent charge mobility, and loosens the fullerene aggregation networks to facilitate exciton dissociation. The efficient Förster energy transfer from PCDTBT8 to PffBT4T-2OD enables the ternary devices to retain a high short-circuit current despite the slightly decreased light absorption. Device physics studies suggest that the addition of PCDTBT8 can enhance the built-in voltage, prolong the carrier lifetime, reduce the defect density and suppress the trap-assisted charge recombination, leading to an improved FF and V_{OC} to enhance the efficiency of ternary devices.

Keywords: polymer solar cells, ternary solar cells, morphology, device physics

1. Introduction

Efforts from the synthesis of new small-bandgap polymers^{1,2}, morphological control^{3,4}, interfacial engineering^{5,6} and device architectural design^{7,8} have driven a steady progress of polymer solar cells (PSCs) with the maximum power conversion efficiency (PCE) now approaching 14%⁹. For the fullerene-based PSCs, empirical experience has led current studies to focus on the use of narrow bandgap conjugated polymers to obtain high J_{SC} values, and electron-donors with deep HOMO energy levels to get a high V_{OC} . However, a sizeable challenge must be overcome in order to further push forward the efficiency limit of PSCs, which is the trade-off between the highest short-circuit current (J_{SC}) and open-circuit voltage (V_{OC}) that can be simultaneously achieved by incorporating a singular photovoltaic blend in a single junction device, as a result of thermalization losses and the Shockley-Queisser efficiency limit¹⁰.

Although connecting two operational sub-devices with complementary absorption ranges in series to build a tandem device is a smart way to enhance the light absorption, it is complicated to assemble and the costly fabrication process hinders the large-scale production.¹¹ In contrast, fabricating ternary solar cells (TSCs) is a promising strategy to broaden the absorption spectrum without introducing sophisticated processing procedures. Recently, several research efforts aimed at increasing the PCE of TSCs by introducing a third component to either broaden light harvesting^{12,13}, encourage energy¹⁴ and charge transfer¹⁵, optimize morphology^{16,17} or achieve a thick active layer^{18,19}, have led to a notable PCE of 14% in TSCs²⁰. To design TSCs with improved efficiency over their binary counterparts, a few criteria need to be met for a positive impact. Firstly, the third component need to have some miscibility with the primary components, so it can locate either in the primary donor or acceptor phases, at the donor/acceptor interface, or form new alloys²¹. Secondly, rational energy or charge transfer to a component that has more efficient charge dissociation or transport ability would improve the device performance²². Multi-length scale (hierarchical) morphology with the coexistence of big and small domains have been found in a large number of fullerene and non-fullerene PSCs, and achieving a high average purity and highly ordered packing at the smallest length scale have been found to facilitate efficient exciton splitting and charge transport.^{23,24,25} Admittedly, some ternary PSC systems also suffer from the trade-off between fill factor (FF), J_{SC} and V_{OC} . Although some high performing TSCs have been realized with increased FF and J_{SC} , their V_{OC} have been pinned to the smaller V_{OC} of the corresponding binary blends²⁶.

Compared to other narrow bandgap polymers, poly[(5,6-difluoro-2,1,3-benzothiadiazol-4,7-diyl)-alt-(3,3'-di(2-octyldodecyl)-2,2';5',2'';5'',2'''-quaterthiophen-5,5'''-diyl)] (PffBT4T-2OD) is a crystallizable polymer that has high hole mobility with strong temperature-dependent aggregation behavior, which can be manipulated to form an ideal polymer:fullerene morphology with highly crystalline and small polymer domains^{27,28}. This has enabled high J_{SC} and FF values to be achieved even in thick PffBT4T-2OD:PC₇₁BM films of 300 nm, with a PCE over 10%. Although previous works have reported that PffBT4T-2OD can be selected as a second electron donor to facilitate ideal morphology to improve the PCE of TSCs^{29,30}, TSCs with PffBT4T-2OD as the host electron donor to take advantage of its favorable photovoltaic properties to achieve even higher PCEs have so far not been reported in the literature.

In this study, we introduce a medium bandgap polymer, namely poly[9-(heptadecan-9-yl)-9H-carbazole-2,7-diyl-alt-(5,6-bis(octyloxy)-4,7-di(thiophen-2-yl)benzo[c][1,2,5]thiadiazole)-5,5-diyl] (PCDTBT8), as the third component into the binary PffBT4T-2OD:PC₇₁BM photovoltaic system to prepare TSCs. The highest occupied molecular orbital (HOMO) energy level of PCDTBT8 is lower than that of PffBT4T-2OD (see Figure 1c)³¹, so it has the potential to increase the V_{oc} of TSCs. The molecular packing in PCDTBT8 won't be changed at a relatively high thermal-annealing temperature around 100 °C, therefore the necessary hot annealing procedure of PffBT4T-2OD:PC₇₁BM system shall not introduce any negative impacts to the device performance of TSCs. Our results show that the Förster energy transfer from PCDTBT8 to PffBT4T-2OD makes the ternary devices retain high short-circuit currents despite a slight decrease of light absorption of the ternary blends. The good miscibility of PCDTBT8 with PC₇₁BM and its location at the interface between PffBT4T-2OD and PC₇₁BM facilitate excellent exciton dissociation and charge transfer characteristics in the ternary blend. Furthermore, device physics investigations suggest that the addition of PCDTBT8 can enhance the built-in voltage, prolong the carrier lifetime, reduce the defect density, and suppress the trap-assisted monomolecular recombination. As a result, the ternary device with the addition of 15 wt.% PCDTBT8 achieved a high PCE of 11.2% with a V_{oc} of 0.79 V, J_{SC} of 18.8 mA cm⁻² and FF of 74.7%.

2. Results and discussion

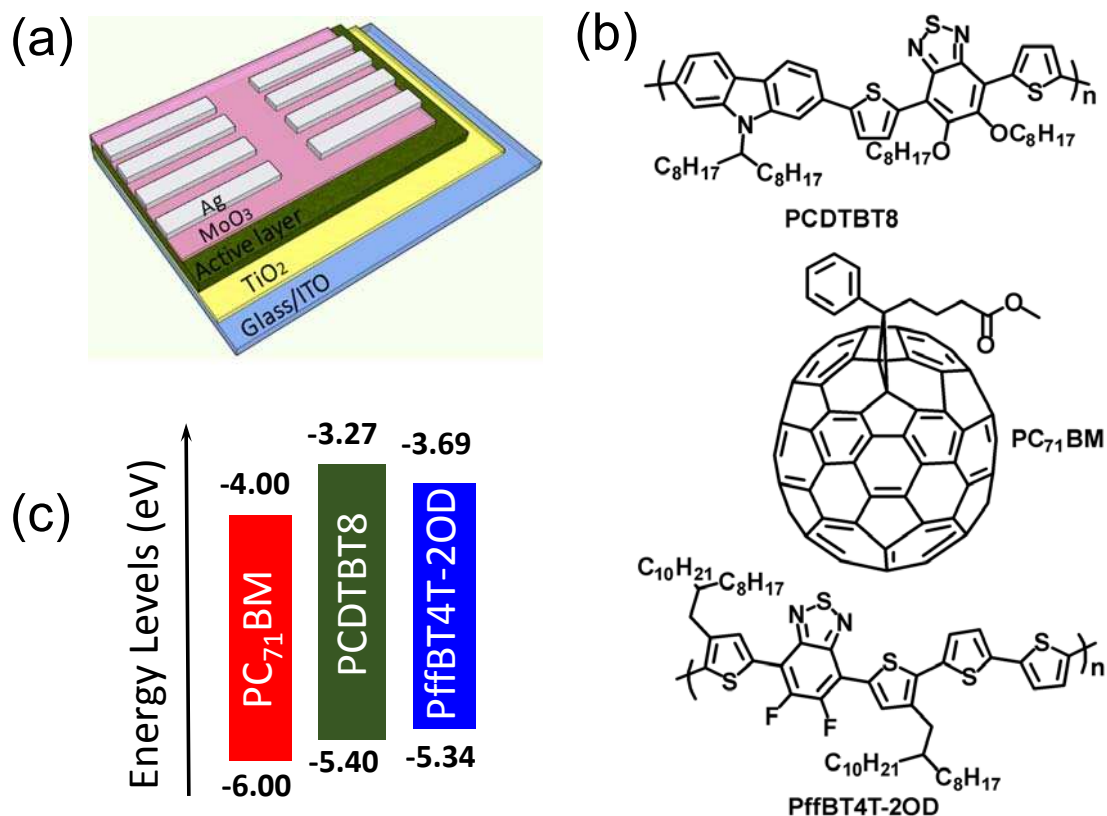


Figure 1 (a) Device architecture of the ternary PSCs. (b) The chemical structures and (c) energy levels of PffBT4T-2OD, PCDTBT8 and PC₇₁BM.

All devices in this work were fabricated in an inverted configuration of ITO/TiO₂/PffBT4T-2OD:PCDTBT8:PC₇₁BM/MoO₃/Ag (see Figure 1). Figures 1b and c show the chemical structures and energy levels of PCDTBT8, PffBT4T-2OD and PC₇₁BM^{29,32}. The HOMO energy level of PCDTBT8 is -5.40 eV, which is deeper than that of PffBT4T-2OD at -5.34 eV, therefore the incorporation of PCDTBT8 has the potential to improve the V_{OC} of our TSCs. PffBT4T-2OD is a crystalline polymer²⁹, whilst PCDTBT8 is amorphous³³. Figure 2 shows the transmission electron microscopy (TEM) of PffBT4T-2OD:PC₇₁BM, PCDTBT8:PC₇₁BM and PffBT4T-2OD:PCDTBT8:PC₇₁BM films. The dark and bright regions represent the fullerene and polymer domains respectively due to their different electron densities³⁴. It can be seen from Figure 2a and b that the PffBT4T-2OD:PC₇₁BM blend film consists of fibril-like textured domains that we identify as the semi-crystalline polymer PffBT4T-2OD, whilst PCDTBT8:PC₇₁BM exhibits a homogeneous distribution of donor and acceptor. With the introduction of PCDTBT8 into the PffBT4T-2OD:PC₇₁BM host blend, the fibril-like textures are retained which is favorable for carrier

transfer, although in these ternary blends the fibrils coalesced together to have slightly larger but more continuous polymer (bright) and fullerene (dark) domains (see Figure 2c-e).

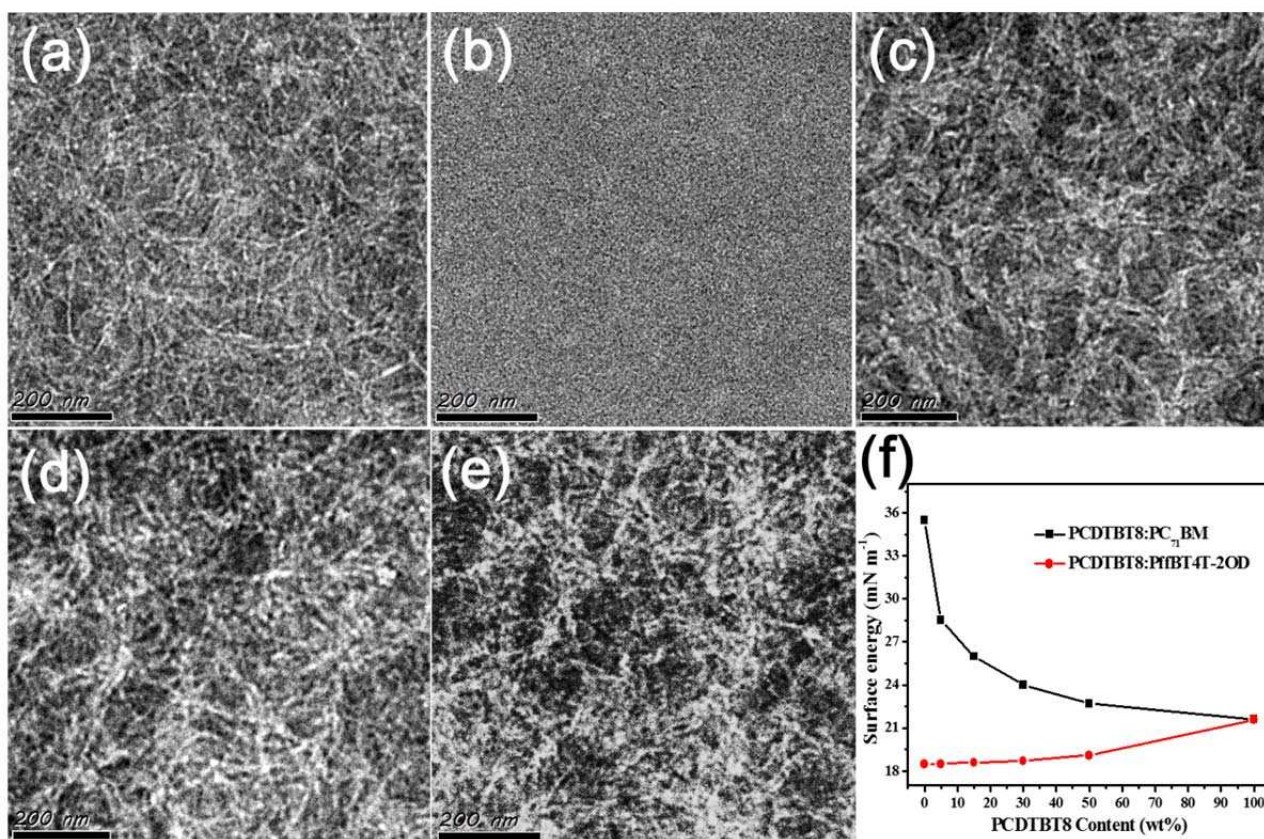


Figure 2 TEM images of the binary and ternary films. (a) PffBT4T-2OD:PC₇₁BM (1:1.2). (b) PCDTBT8:PC₇₁BM (1:4). PffBT4T-2OD:PCDTBT8:PC₇₁BM ternary films with the blending ratios of (c) 0.95:0.05:1.2, (d) 0.85:0.15:1.2 and (e) 0.7:0.3:1.2. (f) Surface energies of PCDTBT8:PC₇₁BM and PCDTBT8:PffBT4T-2OD binary blend films with the presence of different amounts of PCDTBT8.

We have attempted to identify the location of PCDTBT8 within the ternary photovoltaic blends via a surface energy analysis approach, where the localization of the third component in a ternary blend can be inferred from the interfacial surface energy and wetting coefficient of the third component³⁵. The surface energies of pure PffBT4T-2OD, PC₇₁BM and their blend films with the presence of different amounts of PCDTBT8 were estimated from the water contact angle (WCA) measurements and are summarized in Table S1. The surface energy of PCDTBT8 ($\gamma_{\text{PCDTBT8}} = 21.6 \text{ mJ cm}^{-2}$) was observed to be between those of PffBT4T-2OD ($\gamma_{\text{PffBT4T-2OD}} = 18.5 \text{ mJ cm}^{-2}$) and PC₇₁BM ($\gamma_{\text{PC71BM}} = 35.5 \text{ mJ cm}^{-2}$). As reported in previous work³⁶, the closeness of the surface energy values of the electron-donating polymers ensures good miscibility in ternary systems. Figure

2f shows the surface energies of PffBT4T-2OD and PC₇₁BM films blended with various contents of PCDTBT8. We found that the surface energy $\gamma_{PC_{71}BM:PCDTBT8}$ decreased whilst the surface energy $\gamma_{PffBT4T-2OD:PCDTBT8}$ increased monotonically with the addition of PCDTBT8. The interfacial surface energies between different materials within the ternary blend were calculated using equation 1 in the supporting information and are summarized in Table S2. The wetting coefficient of PCDTBT8 in PffBT4T-2OD:PC₇₁BM was calculated to be 0.6 using equation 2 in the supporting information, this value is less than unit and has been concluded to indicate that PCDTBT8 primarily locates at the interface between PffBT4T-2OD and PC₇₁BM domains³⁷.

We have further qualified the crystallization of PffBT4T-2OD and the domain changes of the ternary TSCs via grazing incidence small-angle X-ray scattering (GISAXS). The 2D GISAXS patterns of the binary PffBT4T-2OD:PC₇₁BM blend film and ternary films with 5, 15 and 30 wt. % of PCDTBT8 are shown in Figure 3 a-d. The broad q range of our GISAXS setup also allows the (100) lamellae diffraction ring in the out-of-plane direction to be displayed together with the 2D GISAXS patterns, whose appearance supports our earlier identification of the fibril-like texture to be the crystallizable PffBT4T-2OD component. The location of this (100) pattern is at $q \approx 0.28 \text{ \AA}^{-1}$ from the 1D profile plotted in Figure 3e, and is consistent with previous reports^[9,10]. The domain size of the polymer crystallites at (100) (D_{100}) are calculated by Scherrer's relation and shown in Table 1³⁸. It is clear that the intensity and full width at half maximum of the lamellae (100) diffraction peaks are unchanged, suggesting that the addition of PCDTBT8 did not alter the crystallinity of PffBT4T-2OD in the ternary system. Investigation of the π - π stacking peak of PffBT4T-2OD upon the addition of PCDTBT8 also suggests negligible modifications. Figure 3f plots the in-plane 1D profiles extracted at the specular beam position within the region $q_y = 0 \pm 0.002 \text{ \AA}^{-1}$. The profiles were fitted with a universal model (described in detail in the supporting information)^{39,40}. The fitting parameters are summarized in Table 1, in which ξ is the average correlation length of the PC₇₁BM dispersed polymer-rich phase, η and D are the correlation length and fractal dimension of the fractal-like network of PC₇₁BM, $2Rg$ is the product of η and D which represents the length of the clustered PC₇₁BM domain. It should be noted that the PC₇₁BM dispersed polymer-rich phase contains both crystalline and amorphous PffBT4T-2OD molecules with dispersed PC₇₁BM particles. The binary PffBT4T-2OD:PC₇₁BM film showed the smallest correlation length of the PC₇₁BM dispersed polymer (43.4 nm) and clustered PC₇₁BM (18.2 nm) domains, in line with literature work^{41,42}. The fullerene-dispersed polymer domain size and

fullerene cluster size only show a minor increase with the addition of 5 and 15 wt. % PCDTBT8, as seen in Table 1, further demonstrating that PCDTBT8 did not significantly disrupt the morphology of the host blend. The domain size (D100) of the crystalline polymer was unchanged and the correlation length of the PC₇₁BM dispersed polymer-rich phase (ξ) increased with the addition of PCDTBT8, implying that the increased ξ originates from the mixed PCDTBT8:fullerene fraction. Furthermore, with the incorporation of PCDTBT8, the fractal dimension of fullerene fractal networks decreased from 2.9 to 2.7 but the domain size extended from 17.8 to 22.3 nm, suggesting that the PCBM clusters became loose³³. Based on the above morphological investigation of the TSC film, we schematically show the microstructure of the binary and ternary blends in Figure 3g and h. The PCDTBT8 component is largely located at the interface between PffBT4T-2OD and PC₇₁BM domains, while its good miscibility with PC₇₁BM allows it to diffuse into the PC₇₁BM aggregation to dilute PCBM clusters, leading to a loosely-packed fullerene network. As reported in previous work, these loosely-packed fractal fullerene networks can extend to larger regions to facilitate exciton dissociation⁴³.

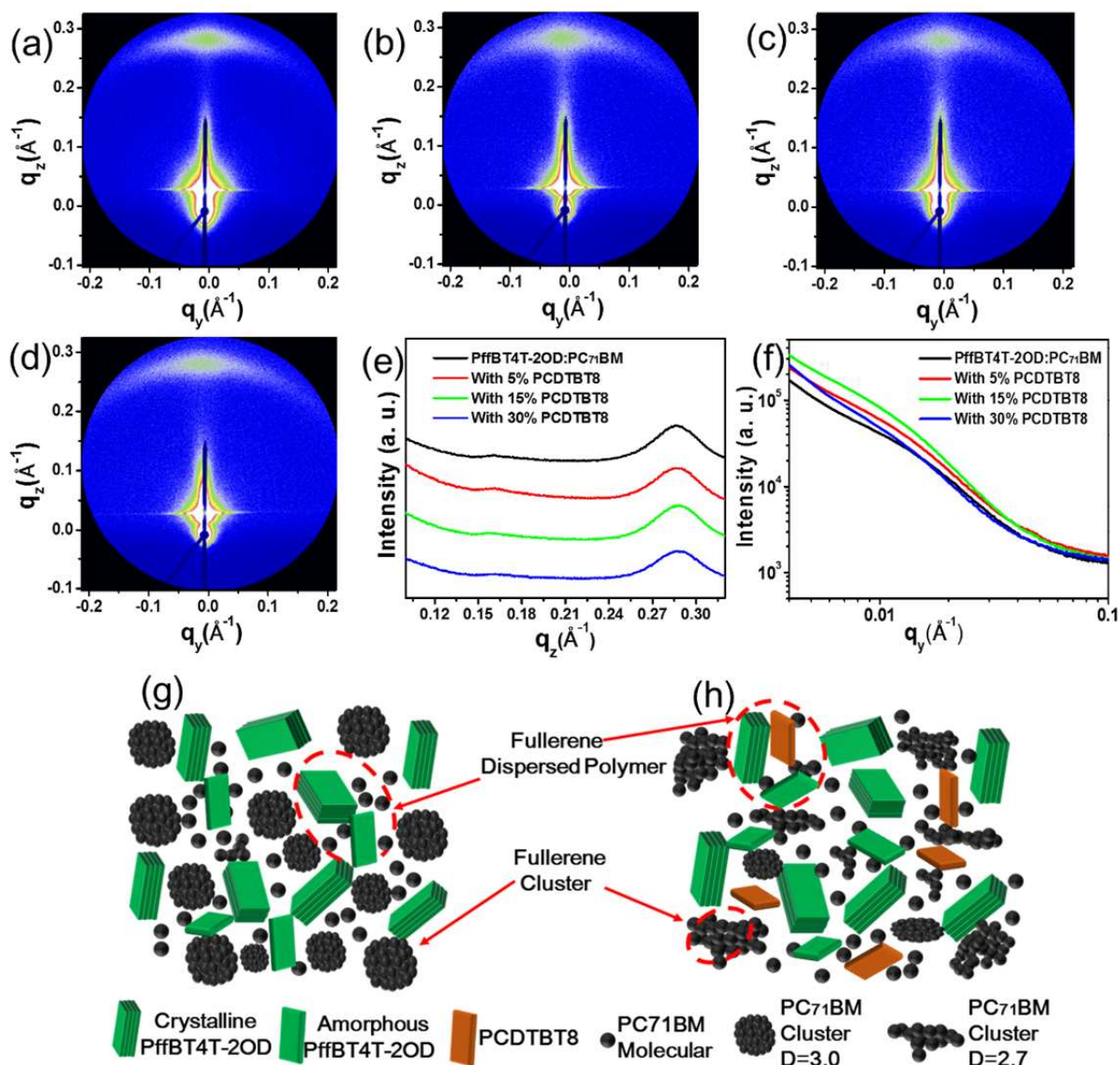


Figure 3 2D GISAXS patterns of (a) PffBT4T-2OD:PC₇₁BM, and its ternary blends with (b) 5, (c) 15 and (d) 30 wt% PCDTBT8. (e) 1D GISAXS profiles along q_z axis showing the (100) diffraction peak of PffBT4T-2OD. (f) 1D GISAXS profiles along q_y axis. Schematic of the microstructure of the PffBT4T-2OD:PC₇₁BM based (g) binary and (h) ternary blend films.

Table 1 Fitting parameters of 1D GISAXS profiles of PffBT4T-2OD:PC₇₁BM based binary and ternary films.

	D_{100} [nm]	ζ [nm]	η [nm]	D	$2R_g$ [nm]
PffBT4T-2OD:PC ₇₁ BM	15.7	43.4	7.5	3.0	17.8
With 5% PCDTBT8	15.7	45.5	8.0	2.8	18.4
With 15% PCDTBT8	15.7	47.4	8.5	2.8	20.3
With 30% PCDTBT8	15.7	54.9	9.1	2.7	22.3

The UV-Vis absorption spectra of PffBT4T-2OD:PC₇₁BM binary and ternary films with different contents of PCDTBT8 are shown in Figure 4a. The addition of PCDTBT8 caused the absorption ability to decrease in the 550 to 700 nm range but increase in the 350 to 550 nm range, indicating that the introduced PCDTBT8 slightly reduces the amount of the absorbed photons and may lead to a reduced J_{SC} in TSCs. Figure S1 shows the emission and absorption spectra of PffBT4T-2OD:PCDTBT8 binary and ternary film with different amount of PCDTBT8. It shows that the maximum absorption peaks of PffBT4T-2OD are located from 600 to 750 nm while, in contrast, this range contains the maximum PL emission peaks of PCDTBT8. These overlapped absorption and PL emission spectra can offer an efficient Förster-type energy transfer^{44,45} in the ternary blend. As shown in figure S1b, the PL intensity of PffBT4T-2OD gradually increases upon blending with PCDTBT8, whilst the PL of PCDTBT8 is quenched completely, implying efficient energy transfer from PCDTBT8 to PffBT4T-2OD⁴⁶. The possibility of charge transfer between PffBT4T-2OD and PCDTBT8 was also investigated by measuring the J-V curves of PffBT4T-2OD:PCDTBT8 binary devices with varying blending ratios. As shown in Figure S2, it is apparent that the binary solar cells with 50% PffBT4T-2OD and 50% PCDTBT8 show a low J_{SC} value between pure PffBT4T-2OD and pure PCDTBT8 solar cells, illustrating that the exciton dissociation at the PffBT4T-2OD/PCDTBT8 interface is negligible and therefore there is no effective charge transfer between them²¹.

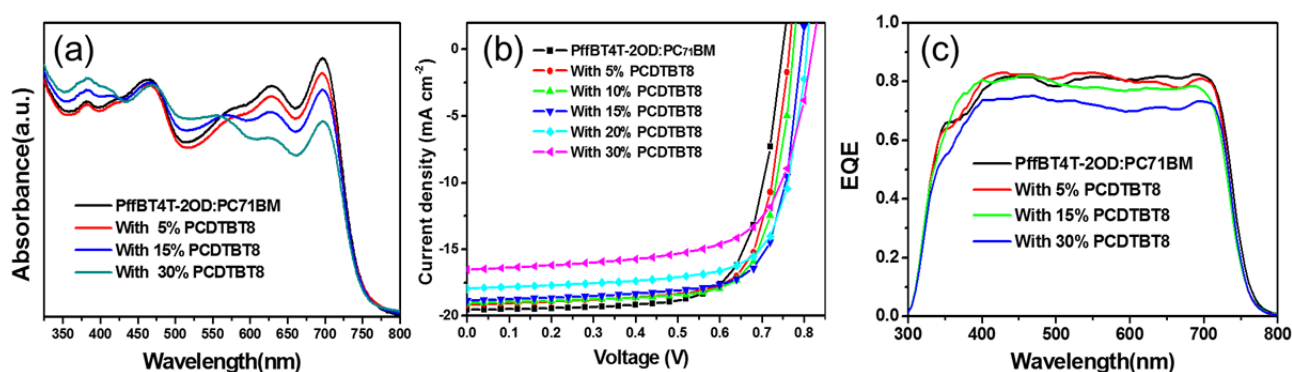


Figure 4 (a) The absorption spectra of PffBT4T-2OD:PC₇₁BM blends with different amounts of PCDTBT8. (b) Champion J–V curves of ternary PSCs with different PCDTBT8 contents. The weight ratio of electron-donating polymers to PC₇₁BM was fixed at 1:1.2. (c) Corresponding EQE spectra of the ternary PSCs.

Table 2 Summary of photovoltaic parameters of inverted ternary solar cells with different contents of PCDTBT8 under the illumination of AM 1.5G at 100 mW cm⁻². The overall donors to PC₇₁BM ratios were kept at 1:1.2. The data presented are the maximum values followed by average values and standard deviations in the parentheses, obtained from over 20 individual devices.

Component	Voc [V]	Jsc [mA cm ⁻²]	FF [%]	PCE [%]
PffBT4T-2OD:PC ₇₁ BM	0.75 (0.75 ± 0.01)	19.5 (19.2 ± 0.3)	72.2 (71.8 ± 0.6)	10.57 (10.3 ± 0.12)
With 5% PCDTBT8	0.76 (0.76 ± 0.01)	19.2 (18.9 ± 0.4)	74.3 (74.1 ± 0.8)	10.89 (10.7 ± 0.08)
With 10% PCDTBT8	0.77 (0.77 ± 0.01)	19.0 (18.5 ± 0.4)	75.1 (74.9 ± 1.1)	11.07 (10.9 ± 0.08)
With 15% PCDTBT8	0.79 (0.79 ± 0.01)	18.8 (18.4 ± 0.4)	74.7 (74.5 ± 0.8)	11.17 (11.0 ± 0.10)
With 20% PCDTBT8	0.81 (0.81 ± 0.01)	17.9 (17.5 ± 0.5)	73.1 (72.2 ± 1.3)	10.56 (10.4 ± 0.07)
With 30% PCDTBT8	0.82 (0.82 ± 0.01)	16.2 (15.8 ± 0.5)	67.1 (66.5 ± 1.1)	9.10 (8.8 ± 0.13)

Figure 4b shows the current density versus voltage (J-V) characteristics. The photovoltaic parameters for TSCs are summarized in Table 2. The PffBT4T-2OD:PC₇₁BM reference device exhibited a best PCE of 10.57%, with a Jsc of 19.5 mA cm⁻², Voc of 0.75 V and FF of 72.2 %. The TSCs exhibited only a moderate decrease in Jsc with the increased PCDTBT8 content, maintaining 83% even with 30 wt% PCDTBT8, despite the decreased absorption intensity detailed earlier. This may be ascribed to the energy transfer from PCDTBT8 to PffBT4T-2OD. Notably, the FF of the TSCs increased from 72.2 to 74.3 and 75.1 % when the weight ratio of PCDTBT8 is 5 and 15% respectively, signifying that the addition of PCDTBT8 may improve the charge mobility or reduce recombination. Additionally, the V_{OC} of our TSCs continuously increased with the increasing content of PCDTBT8, in line with previous reports that the V_{OC} of TSCs can be continuously tuned between the V_{OC} values of corresponding binary solar cells^{47,48}, instead of following the regular rule that V_{OC} will usually be determined by the difference between the LUMO level of acceptor and the lower HOMO level of donors. As a result, TSCs with 15 wt. % PCDTBT8 achieved a maximum PCE of 11.2%, with the V_{OC} of 0.79 V. On the contrary, although TSCs with 30 wt. % PCDTBT8 can obtain a higher V_{OC} of 0.82 V, their J_{SC} and FF declined significantly, leading to a relatively low PCE of 9.1%. It should be noted that the optimized ratio of PffBT4T-2OD to PC₇₁BM is 1:1.2²³, whilst the optimized ratio of PCDTBT8 to PC₇₁BM is 1:4²⁷. We therefore fabricated TSCs with higher ratios of fullerene to polymer. The results are summarized in Table S4, showing that TSCs exhibit an increased FF and a decreased J_{SC} with higher fullerene contents, causing little change in the PCE when the increase of fullerene loading is moderate, and reduced PCE at much higher fullerene loadings. The external quantum efficiency (EQE) curves are shown in Figure 4c, and the

integrated EQE values are consistent with J_{SC} values, showing a slight decline with the addition of PCDTBT8. We have also fabricated a batch of TSC devices with a much larger active area of 8.5 mm^2 , and the device metrics are summarized in Table S5. With the increased active layer area from 2.12 to 8.5 mm^2 , the J_{sc} and FF values decreased slightly due to the increased series resistance whilst the V_{oc} values remains essentially unchanged. Notably, an encouraging PCE of 10.5%, with a V_{oc} of 0.80 V , J_{sc} of 18.3 mA cm^{-2} and FF of 71.7%, was achieved for the device adding 15% PCDTBT8, illustrating that PffBT4T-2OD based TSCs also has the potential to fabricate large-area devices. PffBT4T-2OD:PC₇₁BM binary solar cells have been found to degrade quickly as a result of spinodal demixing of donors and acceptors in the solid state during operation.⁴¹ Our preliminary investigation found that the incorporation of PCDTBT8 slowed down the efficiency degradation rate of our TSCs by reducing the phase separation rate between donors and acceptors. We are performing morphological characterizations and plan to correlate morphological evolution with storage lifetime of those TSCs, and report details in a following-up report.

To understand the influence of PCDTBT8 content on the photovoltaic parameters of TSCs, we have evaluated the exciton dissociation and carrier transport/recombination process. Figure 5a shows the photocurrent density (J_{ph}) as a function of the effective voltage (V_{eff}) of our TSCs. Here, J_{ph} is defined as $J_{ph} = J_{light} - J_{dark}$, where J_{light} and J_{dark} are the photocurrent densities under illumination and dark respectively, and V_{eff} is defined as $V_{eff} = V_0 - V_a$, where V_0 is the voltage when $J_{ph}=0$ and V_a is the applied voltage. The J_{ph} of all devices quickly saturates when V_{eff} approaches 1 V , indicating that all generated electron-hole pairs are dissociated under this condition. As shown in Table S6, the saturated current density (J_{sat}) of TSCs exhibits only a slight decline from 19.9 to 19.2 mA cm^{-2} with the incorporation of 15 wt. % PCDTBT8, suggesting that the generated excitons are nearly unaffected. $P(E, T)$ is determined by normalizing J_{ph} with respect to J_{sat} (J_{ph}/J_{sat}). The $P(E, T)$ of our TSCs with 0, 5, 15 and 30 wt. % of PCDTBT8 are 97.9%, 98.3%, 98.0% and 94.3% respectively, which shows that the exciton dissociation can be enhanced with a moderate addition of PCDTBT8. Furthermore, the hole mobility was measured to investigate the charge transfer of these TSCs. Figure S3 and Table S6 show that although the hole mobilities of TSCs decreases with the addition of PCDTBT8 particularly at higher weight fractions, the TSCs with 5 and 15 wt% PCDTBT8 can acquire a high hole mobility of about $10^{-2} \text{ cm}^2\text{V}^{-1}\text{S}^{-1}$, comparable to that of the binary device. The study of PCDTBT:PC₇₁BM system has concluded that bimolecular recombination dominate the recombination process when the slope in Figure 5b is 1.01 (kT/q) ⁴⁹.

Instead, a signature of monomolecular or trap-assisted recombination will operate with an enhanced dependence of the open circuit on the light intensity ($2kT/q$). As shown in Figure 5b, slopes of 1.16, 1.10, 1.06 and 1.05 kT/q were obtained for the PffBT4T-2OD:PC₇₁BM binary and PffBT4T-2OD:PCDTBT8:PC₇₁BM ternary blends with a blending ratio of 0.95:0.05:1.2, 0.85:0.15:1.2, and 0.7:0.3:1.2 respectively. Indeed, bimolecular recombination dominates in all devices and the trap-assisted monomolecular recombination became weaker with the addition of PCDTBT8. Figure S3b shows the J-V curves of TSCs with different contents of PCDTBT8 under dark conditions. It can be seen that TSCs with 5 and 15 wt. % PCDTBT8 show a relatively low leak current compared to the PffBT4T-2OD:PC₇₁BM device, illustrating that the incorporation of PCDTBT8 could prevent the current leakage to reduce carrier recombination. While their dark currents under the forward bias were almost unchanged with 5 and 15 wt. % PCDTBT8, suggesting that PCDTBT8 did not alter the series resistance of the host blend⁵⁰. However, TSCs with 30 wt. % PCDTBT8 show a low current in the forward direction and high leakage current in the reverse direction, consistent with its poor FF and J_{SC}. Overall, we can conclude that the enhanced FF in our TSCs comes from the enhanced exciton dissociation and reduced carrier recombination, instead of increased carrier transportation.

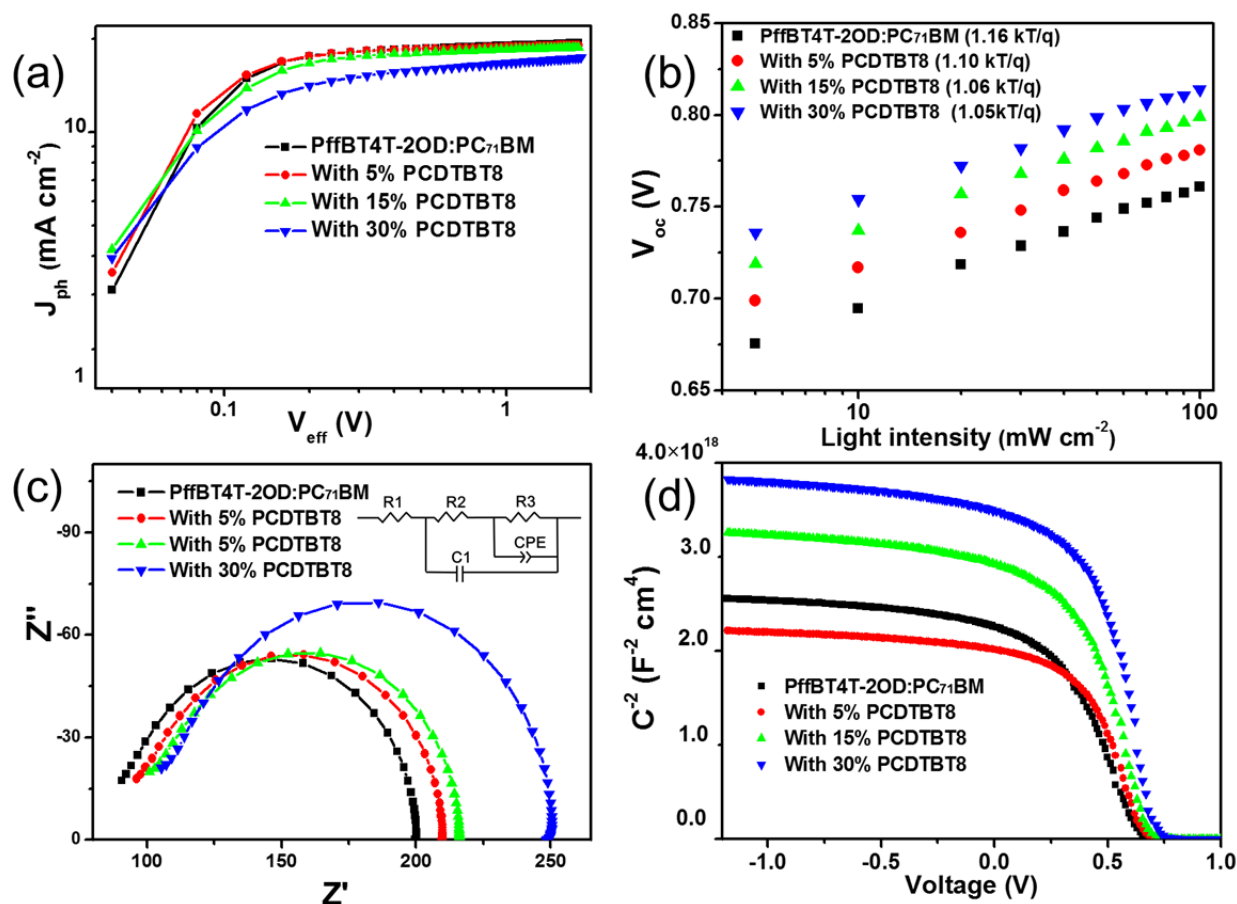


Figure 5 (a) Photocurrent density versus effective voltage curves. (b) V_{OC} versus light intensity with the slope gradient indicated in brackets. (c) Nyquist plots of impedance spectra with an applied bias near V_{OC} under 0.8 sun irradiation. Inset shows the equivalent circuit model to fit the impedance spectra. (d) The Mott-Schottky plot of solar cells measured at a probe frequency of 10 kHz.

Alternating current impedance spectroscopy (IS) was performed to gain in-depth understanding of the charge transport and recombination processes. Figure 5c shows the corresponding Nyquist plots of the binary and ternary solar cells, measured at $V=V_{OC}$ under the illumination of 0.8 Sun and fitted using the equivalent circuit model shown in the inset of Figure 5c. The model contains a series resistance R_1 , coming mainly from the electrical contacts and the resistance of the electrodes, which remained almost constant in all devices (see Table S7). R_2 and R_3 correspond to the transport and recombination resistances of the active layer, which could be used to evaluate the charge carrier transport and recombination processes.⁵¹ Values of R_2 and R_3 from this model fit show that the addition of PCDTBT8 will increase both the transport and recombination resistances of our TSCs, corresponding to the reduced charge transport mobility and suppressed recombination. The constant phase element (CPE) suggests non-ideal behavior of the

capacitor, and is defined by CPE-T and CPE-P⁵², representing the capacitance and an inhomogeneous constant respectively. If CPE-P equals 1, the CPE is identical to an ideal capacitor without the presence of any defects at the polymer:fullerene interface⁵³. Our model fitting shows that the CPE-P of TSCs all increased towards unit with the addition of PCDTBT8, suggesting that the interface capacitance between our electron-donating polymer and electron-accepting fullerene becomes ideal with the introduction of PCDTBT8. Furthermore, the average carrier lifetime (τ) in the active layer can be calculated from the equation: $\tau=R_3 \times \text{CPE-T}$ ⁵⁴, and the τ values are estimated to be 1.61, 2.10, 2.20 and 2.31 μs for devices with 0, 5, 15 and 30 wt% of PCDTBT8 respectively. A longer τ is associated with a lower recombination rate and therefore the addition of PCDTBT8 significantly suppressed the charge recombination in the ternary film.

The V_{OC} of PSCs is empirically determined from the separation between Fermi levels of holes (E_{Fn}) and Fermi levels of electrons (E_{Fp}) using the following equation: $V_{\text{OC}}=(E_{\text{Fn}} - E_{\text{Fp}})/q$ ⁵⁵. In order to explore the dramatic increase of V_{OC} in our TSCs, capacitance-voltage (C-V) measurements were performed and devices were analyzed via the Mott-Schottky (MS) analysis^{56,57}. Table S8 shows the built-in potential (V_{BI}) and defect density (N) of our TSCs, which are calculated from the Mott-Schottky analysis detailed in the supporting information. The V_{BI} of all the TSCs increased with increasing PCDTBT8 content, and the difference between V_{OC} and V_{BI} remained constant for all our TSCs at 0.11 V, indicating that the increased V_{BI} is responsible for the enhanced V_{OC} . In addition, previous work has illustrated that the density of defects dominates over variations in bandgap and will determine the final achievable V_{OC} ⁵⁸. As shown in Table S8 and Figure 6, the defect density of the TSCs decreased from 9.9×10^{14} for the binary device to $8.3 \times 10^{14} \text{ cm}^{-3}$ for the ternary device with 15 wt. % of PCDTBT8. When devices are under illumination, TSCs with a lower defect density will exhibit a larger energy shift than the TSCs with a higher defect density. This is due to fewer electronic states within the bandgap available to be occupied by photo-generated charges, and leads to a deeper downward shift with respect to the equilibrium Fermi level E_{F0} and thus a higher V_{OC} is obtainable.

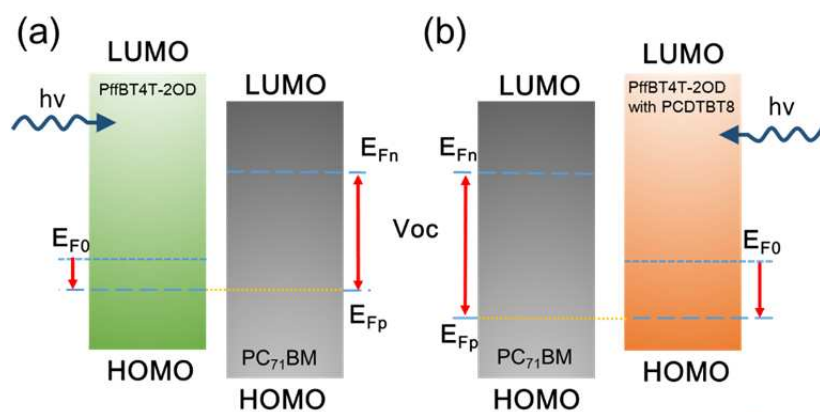


Figure 6 Energy diagrams of the (a) binary and (b) ternary blends under illumination indicating the electrically active states in the bandgap of both materials. The donor HOMO level will be displaced depending on the addition of PCDTBT8. The position of the equilibrium (dark) Fermi level is denoted E_{F0} . The difference between the hole (E_{Fp}) and electron (E_{Fn}) Fermi Levels yields the open-circuit voltage.

3. Conclusion

In summary, we demonstrated that high performance ternary solar cells can be prepared by incorporating a medium band-gap polymer PCDTBT8 into a crystalline PffBT4T-2OD:PC₇₁BM host blend. The third component PCDTBT8 was determined to locate at the interface between PffBT4T-2OD and PC₇₁BM without disrupting the crystallization of the primary electron donor PffBT4T-2OD, maintaining good charge mobility, and was found to loosen the fullerene aggregation networks that lead to superior exciton dissociation. Despite the slightly reduced absorption of ternary devices, the J_{SC} of ternary devices remains at around 83% even with 30 wt% of PCDTBT8, due to efficient energy transfer from PCDTBT8 to PffBT4T-2OD. Device physics studies support that the addition of PCDTBT8 can enhance the built-in voltage, prolong the carrier lifetime, reduce the defect density and suppress the trap-assisted charge recombination, leading to an improved FF and V_{OC} . As a result, the ternary device with 15 wt. % PCDTBT8 exhibits a maximum PCE of 11.2% with a V_{OC} of 0.79 V, a J_{SC} of 18.8 mA cm⁻² and FF of 74.7%. Our results suggest that suppressing charge recombination and reducing defect density in ternary blends is an effective approach to improve the performance of PSCs.

4. Experimental Section

4.1. Materials

PffBT4T-2OD and PC₇₁BM were purchased from Solarmer Materials (Beijing) Inc. PCDTBT8 was synthesized in our previous work^{27,42}. TiO₂ nanoparticles were synthesized according to our previous report⁵⁹. Unless otherwise stated, all chemicals and solvents were of reagent grade and used as received.

4.2. Fabrication of ternary solar cells

Solar cells were fabricated in inverted structures. The pre-patterned ITO-glass substrates (resistance *ca.* 15 Ω per square) were cleaned by sequential sonication in water, ethanol, and isopropyl alcohol for 10 minutes each, before drying at 100 °C on a hotplate. After ultraviolet/ozone treatment for 10 min, 20 nm TiO₂ films were cast from the TiO₂ dispersion with the presence of 40 mol% titanium (diisopropoxide) bis(2,4-pentanedionate) (TIPD) by spin-coating at 3000 rpm, followed by thermal annealing at 150 °C for 30 minutes to convert TIPD to titanium oxide bis(2,4-pentanedionate) (TOPD). TOPD here acts as a binder among TiO₂ nanoparticles to reduce morphological and energetic defects, and has been demonstrated as an efficient electron transport layer for organic and perovskite photovoltaics in our previous work⁶⁰. The TiO₂ films were then transferred into an N₂-filled glove box and irradiated for 10 min under a 254 nm UV light before rinsing with ethanolamine (EA) solution (1 wt. % in 2-methoxyethanol) at 3000 rpm. Active layer solutions were prepared in CB/DCB (1:1 volume ratio) with 3% of DIO (PffBT4T-2OD concentration: 9 mg mL⁻¹). To completely dissolve the polymer, the active layer solution was stirred on a hot plate at 100 °C for at least 5 h. Before spin-coating, both the polymer solution and ITO substrate were preheated on a hot plate at \approx 110 °C. Active layers were spin-coated from the warm polymer solution on the preheated substrate in an N₂ glovebox at 800 rpm. The preheated substrates were transferred to the spin coater chuck and the film casting process was completed within 10 s. Then the device substrates were put in a vacuum chamber overnight (\sim 12h). Finally, 10 nm MoO₃ and 100 nm Ag were deposited onto the photoactive layer through shadow masks by thermal evaporation. All the devices were encapsulated with UV-curable epoxy glue and glass slides before taking out from the glove box for device testing.

4.3. Characterization

Film absorption spectra were measured using a UV-Visible spectrophotometer (HITACHI, Japan). Film thickness was measured using a spectroscopic ellipsometer (J. A. Woollam, USA). Water contact angle measurements were performed using a water contact angle measurement system

(Attension Theta Lite), and the surface energy was calculated using the equation of state. The surface morphologies of the active layers were characterized by transmission electron microscopy (TEM) (JEOL, Japan). Device J-V characterization was performed under AM 1.5G (100 mW cm^{-2}) using a Newport 3A solar simulator in air at room temperature. The light intensity was calibrated using a standard silicon reference cell certified by the National Renewable Energy Laboratory (NREL, USA). J-V characteristics were recorded using J-V sweep software developed by Ossila Ltd. (UK) and a Keithley 2612B (USA) source meter unit. An aperture mask was placed over the devices to accurately define a testing area of 2.12 mm^2 on each pixel and to eliminate the influence of stray and wave guided light. External quantum efficiency (EQE) was measured with a Zolix (China) EQE system equipped with a standard Si diode. Impedance measurements were performed on an XM-studio electrochemical workstation (Solartron, U.K.). Equivalent circuit simulations were conducted using the software package ZView 3.1 (Scribner Associate, Inc., USA). Photoluminescence (PL) was obtained using a PL microscopic spectrometer (Flex One, Zolix, China) with a 532 nm CW laser as the excitation source. Synchrotron grazing incidence small-angle X-ray scattering (GISAXS) measurements were conducted using the beamline BL16B1 at the Shanghai Synchrotron Radiation Facility in China.

Acknowledgments

This work was supported by the National Natural Science Foundation of China (Grants No. 21774097, 21504065) and the Fundamental Research Funds for the Central Universities (WUT: 2017-YB-010) of China. H.Y. and A.I. thank financial support from EPSRC via grant EP/I028641/1. T.W. acknowledges support from the Recruitment Program of Global Experts (1000 Talents Plan) of China. All authors thank the beamline BL16B1 crew at Shanghai Synchrotron Radiation Facility (China) for providing the beam time and help during experiments. We also thank Dr. Zhihong Chen (Department of Physics, Wuhan University of Technology) for helping with the GISAXS data analysis.

Reference

-
- 1 W. Zhao, S. Li, H. Yao, S. Zhang, Y. Zhang, B. Yang, J. Hou, *J. Am. Chem. Soc.* 139 (2017) 7148-7151.
 - 2 J. Lee, D. H. Sin, B. Moon, J. Shin, H. G. Kim, M. Kim, K. Cho, *Energy Environ. Sci.* 10 (2017)

247-257.

- 3 Y. Huang, E. J. Kramer, A. J. Heeger, G. C. Bazan, *Chem. Rev.* 114 (2014) 7006-7043.
- 4 Y. Yan, X. Liu, T. Wang, *Adv. Mater.* 29 (2017) 1601674.
- 5 X. Dou, O. Lytken, M. S. Killian, J. Cao, T. Stubhan, M. Turbiez, P. Schmuki, H. P. Steinrück, L. Ding, R. H. Fink, N. Li, C. J. Brabec, *Adv. Energy Mater.* 7 (2017) 1601959.
- 6 P. Cheng, M. Zhang, T. K. Lau, Y. Wu, B. Jia, J. Wang, C. Yan, M. Qin, X. Lu, X. Zhan, *Adv. Mater.* 29 (2017) 1605216.
- 7 M. Li, K. Gao, X. Wan, Q. Zhang, B. Kan, R. Xia, F. Liu, X. Yang, H. Feng, W. Ni, Y. Wang, J. Peng, H. Zhang, Z. Liang, H. L. Yip, X. Peng, Y. Cao, Y. Chen, *Nat. Photonics* 11 (2017) 85-90.
- 8 J. Huang, H. Wang, K. Yan, X. Zhang, H. Chen, C. Z. Li, J. Yu, *Adv. Mater.* 29 (2017) 1606729.
- 9 Y. Cui, H. Yao, B. Gao, Y. Qin, S. Zhang, B. Yang, C. He, B. Xu, J. Hou, *J. Am. Chem. Soc.* 139 (2017) 7302-7309.
- 10 W. Shockley, H. J. Queisser, *J. Appl. Phys.* 32 (1961) 510-519.
- 11 W. Liu, S. Li, J. Huang, S. Yang, J. Chen, L. Zhao, M. Shi, X. Zhan, C. Z. Li, H. Chen, *Adv. Mater.* 28 (2016) 9729-9734.
- 12 L. Ke, J. Min, M. Adam, N. Gasparini, Y. Hou, J. D. Perea, W. Chen, H. Zhang, S. Fladischer, A. C. Sale, E. Spiecker, R. R. Tykwinski, C. J. Brabec, T. Ameri, *Adv. Energy Mater.* 6 (2016) 1502355.
- 13 H. Benten, T. Nishida, D. Mori, H. Xu, H. Ohkita, S. Ito, *Energy Environ. Sci.* 9 (2016) 135-140.
- 14 B. Xia, L. Yuan, J. Zhang, Z. Wang, J. Fang, Y. Zhao, D. Deng, W. Ma, K. Lu, Z. Wei, *J. Mater. Chem. A* 5 (2017) 9859-9866.
- 15 S. Liu, P. You, J. Li, J. Li, C. S. Lee, B. S. Ong, C. Surya, F. Yan, *Energy Environ. Sci.* 8 (2015) 1463-1470.
- 16 Y. Zhang, D. Deng, K. Lu, J. Zhang, B. Zhang, Y. Zhao, J. Fang, Z. Wei, *Adv. Mater.* 27 (2015) 1071-1076.
- 17 T. Kumari, S. M. Lee, S. H. Kang, S. Chen, C. Yang, *Energy Environ. Sci.* 10 (2017) 258-265.
- 18 G. Zhang, K. Zhang, Q. Yin, X. F. Jiang, Z. Wang, J. Xin, W. Ma, H. Yang, F. Huang, Y. Cao, *J. Am. Chem. Soc.* 139 (2017) 2387-2395.
- 19 N. Gasparini, L. Lucera, M. Salvador, M. Prosa, George D. Spyropoulos, P. Kubis, H. J. Egelhaaf, C. J. Brabec, T. Ameri, *Energy Environ. Sci.* 10 (2017) 885-892.
- 20 W. Zhao, S. Li, S. Zhang, X. Liu, J. Hou, *Adv. Mater.* 29 (2017) 1604059.
- 21 Y. M. Yang, W. Chen, L. Dou, W. H. Chang, H. S. Duan, B. Bob, G. Li, Y. Yang, *Nat. Photonics*, 9 (2015):190-198.

-
- 22 Q. An, F. Zhang, J. Zhang, W. Tang, Z. Deng, B. Hu, *Energy Environ. Sci.* 9 (2016) 281-322.
- 23 K. Gao, J. Miao, L. Xiao, W. Deng, Y. Kan, T. Liang, C. Wang, F. Huang, J. Peng, Y. Cao, F. Liu, T. P. Russell, H. Wu, X. Peng, *Adv. Mater.* 28 (2016) 4727-4733.
- 24 L. Ye, W. Zhao, S. Li, S. Mukherjee, J. H. Carpenter, O. Awartani, X. Jiao, J. Hou, H. Ade, *Adv. Energy Mater.* 7 (2017) 1602000.
- 25 L. Ye, Y. Xiong, S. Li, M. Ghasemi, N. Balar, J. Turner, A. Gadisa, J. Hou, B. T. O'Connor, H. Ade, *Adv. Funct. Mater.* 27 (2017) 1702016.
- 26 R. A. Street, D. Davies, P. P. Khlyabich, B. Burhart, B. C. Thompson, *J. Am. Chem. Soc.* 135 (2013) 986-989.
- 27 Liu Y, Zhao J, Li Z, C. Mu, W. Ma, H. Hu, K. Jiang, H. Lin, H. Ade, H. Ye, *Nat. Commun.* 5 (2014) 5293.
- 28 W. Ma, G. Yang, K. Jiang, J. H. Carpenter, Y. Wu, X. Meng, T. McAfee, J. Zhao, C. Zhu, C. Wang, H. Ade, H. Yan, *Adv. Energy Mater.* 5 (2015) 1501400.
- 29 X. Liu, J. Wang, J. Peng, Z. Liang, *Macromolecules*, 50 (2017) 6954-6960.
- 30 F. Zhao, Y. Li, Z. Wang, Y. Yang, Z. Wang, G. He, J. Zhang, L. Jiang, T. Wang, Z. Wei, W. Ma, B. Li, A. Xia, Y. Li, C. Wang, *Adv. Energy Mater.* 7 (2017) 1602552.
- 31 H. Yi, S. Al-Faifi, A. Iraqi, D. C. Watters, J. Kingsley, D. G. Lidzey, *J. Mater. Chem.* 21 (2011) 13649-13656.
- 32 A. A. B. Alghamdi, D. C. Watters, H. Yi, S. Al-Faifi, M. S. Almeataq, D. Coles, J. Kingsley, D. G. Lidzey, Ahmed Iraqi, *J. Mater. Chem. A* 1 (2013) 5165-5171.
- 33 T. Wang, N. W. Scarratt, H. Yi, A. D. F. Dunbar, A. J. Pearson, D. C. Watters, T. S. Glen, A. C. Brook, J. Kingsley, A. R. Buckley, M. W. A. Skoda, A. M. Donald, R. A. L. Jones, A. Iraqi, D. G. Lidzey, *Adv. Energy Mater.* 3 (2013) 505-512.
- 34 F. Liu, W. Zhao, J. R. Tumbleston, C. Wang, Y. Cu, D. Wang, A. L. Briseno, H. Ade, T. P. Russell, *Adv. Energy Mater.* 4 (2014) 6706-6714.
- 35 S. Honda, H. Ohkita, H. Benten, S. Ito, *Adv. Energy Mater.* 1 (2011) 588-598.
- 36 N. S. Gobalasingham, S. Noh, J. B. Howard, B. C. Thompson, *ACS Appl. Mater. Interfaces* 8 (2016) 27931-27941.
- 37 J. S. Huang, T. Goh, X. Li, M. Y. Sfeir, E. A. Bielinski, S. Tomasulo, M. L. Lee, N. Hazeri, A. D. Taylor, *Nat. Photonics* (7) 2013 479-485.
- 38 M. Y. Chiu, U. S. Jeng, C. H. Su, K. S. Liang, K. H. Wei, *Adv. Mater.* 20 (2008) 2573-2578.
- 39 J. Mai, T. K. Lau, J. Li, S. H. Peng, C. S. Hsu, U. S. Jeng, J. Zeng, N. Zhao, X. Xiao, X. Lu, *Chem. Mater.* 28 (2016) 6186-6195.
- 40 H. C. Liao, C. S. Tsao, Y. T. Shao, S. Y. Chang, Y. C. Huang, C. M. Chuang, T. H. Lin, C. Y.

-
- Chen, C. J. Su, U. S. Jeng, Y. F. Chen, W. F. Su, *Energy Environ. Sci.* 6 (2013) 1938-1948.
- 41 N. Li, J. D. Perea, T. Kassar, M. Richter, T. Heumueller, G. J. Matt, Y. Hou, N. S. Guldal, H. Chen, S. Chen, S. Langner, M. Berlinghof, T. Unruh, C. J. Brabec, *Nat. Commun.* 8 (2017) 14541.
- 42 Y. Zhang, A. J. Parnell, F. Pontechiani, J. F. K Cooper, R. L Thompson, R. A. L. Jones, S. M. King, D. G. Lidzey, G. Bernardo, *Sci. Rep.* 7 (2017) 44269.
- 43 H. C. Liao, C. S. Tsao, T. H. T. H. Lin, C. M. Chuang, C. Y. Chen, U. S. Jeng, C. H. Su, Y. F. Chen, W. F. Su, *J. Am. Chem. Soc.* 133 (2011) 13064-13073.
- 44 L. Lu, W. Chen, T. Xu, L. Yu, *Nat. Commun.* 6 (2015) 7327.
- 45 V. Gupta, V. Bharti, M. Kumar, S. Chand, A. L. Heeger, *Adv. Mater.* 27 (2015) 4398-4404.
- 46 Q. An, F. Zhang, Q. Sun, M. Zhang, J. Zhang, W. Tang, X. Yin, Z. Deng, *Nano Energy* 26 (2016) 180-191.
- 47 P. P. Khlyabich, B. Burkhart, B. C. Thompson, *J. Am. Chem. Soc.* 134 (2012) 9074-9077.
- 48 Y. Chen, P. Ye, X. Jia, W. Gu, X. Xu, X. Wu, J. Wu, F. Liu, Z. G. Zhu, H. Huang, *J. Mater. Chem. A* 5 (2017) 19697-19702.
- 49 W. L. Leong, S. R. Cowan, A. J. Heeger, *Adv. Energy Mater.* 1 (2011) 517-522.
- 50 A. K. K. Kyaw, D. H. Wang, V. Gupta, J. Zhang, S. Chand, G. C. Bazan, A. J. Heeger, *Adv. Mater.* 25 (2013) 2397-2402.
- 51 B. Xiao, M. Zhang, J. Yan, G. Luo, K. Gao, J. Liu, Q. You, H. B. Wangm, C. Gao, B. Yao, X. Zhao, H. Wu, F. Liu, *Nano Energy* 39 (2017) 478-488.
- 52 G. Perrier, R. Bettignies, S. Berson, N. Lemaitre, S. Guillerez, *Sol. Energy Mat. & Sol. C.* 101 (2012) 210-216.
- 53 A. Sacco, *Renew. & Sust. Energy Rev.* 79 (2017) 814-829.
- 54 T. M. Clarke, C. Lungenschmied, J. Peet, N. Drolet, A. J. Mozer, *Adv. Energy Mater.* 5 (2015) 1401345.
- 55 M. C. Scharber, D. Mühlbacher, M. Koppe, P. Denk, C. Waldauf, A. J. Heeger, and C. J. Brabec, *Adv. Mater.* 18 (2006) 789-794.
- 56 H. Zhou, Y. Zhang, J. Seifert, S. D. Collins, C. Luo, G. C. Bazan, T. Q. Nguyen, A. J. Heeger, *Adv. Mater.* 25 (2013) 1646-1652.
- 57 T. Kirchartz, W. Gong, S. A. Hawks, T. Agostinelli, R. C. I. MacKenzie, Y. Yang, J. Nelson, *J. Phys. Chem. C* 116 (2012) 7672-7680.
- 58 T. S. Ripolles, A. Guerrero, G. Garcia-Belmonte, *Appl. Phys. Lett.* 103 (2013) 236.
- 59 Y. Yan, F. Cai, L. Yang, J. Li, Y. Zhang, F. Qin, C. Xiong, Y. Zhou, D. G. Lidzey, T. Wang, *Adv. Mat.* 29 (2017) 1604044.
- 60 F. Cai, L. Yang, Y. Yan, J. Zhang, F. Qin, D. Liu, Y. B. Chen, Y. H. Zhou, T. Wang, *J. Mater.*



Wei Li was born in 1992. He received a B.S. degree in Materials science and Engineering from Jinan University in 2013 and an M.S. degree in Materials Science and Engineering from Wuhan University of Technology in 2016. He is currently a Ph.D. candidate with a specific focus on polymer solar cells.



Jinlong Cai was born in 1994 in Nantong, China. He received a B.S. degree in Polymer Materials and Engineering from Hubei University of Technology in 2016. He is currently an M.S. student working on organic photovoltaics.



Feilong Cai was born in 1993. He received a B.S. degree in Polymer Materials and Engineering from Wuhan University of Technology in 2015. He is currently an M.S. student working on photovoltaics, with a specific focus on various electron/hole transport materials.



Yu Yan was born in 1991. He received a B.S. degree in Polymer Materials and Engineering and an M.S. degree in Materials Science, from Wuhan University of Technology in 2012 and 2014 respectively. He is currently a Ph.D. candidate majoring in material sciences under the direction of Professor Tao Wang, and his research focuses on improving the power conversion efficiency of organic solar cells via rational morphology control.



Dr. Hunan Yi received his MSc from Shanghai China, and his PhD from University of St Andrews on Dye-Sensitised Solar Cells, where he remained as a research fellow after PhD until 2004. He then became a postdoctoral research associate at the University of Sheffield, developing various conjugated polymers for organic solar cell applications. Since 2015, he is a Knowledge Transfer Account (KTA) associate with both the University of Sheffield and Ossila Ltd. UK.



Dr. Robert Gurney received his PhD in Physics from the University of Surrey in 2013 under the supervision of Professor Joe Keddie. He spent a further 6 months in the same group as a post-doc, working with industrial partners on moisture analysis and scanning probe microscopy of polymer films, before moving to ESPCI in Paris. There, he worked on the adhesion and rheology of SBR at short time scales with Profs. Costantino Creton and Anke Lindner, collaborating with Michelin. He joined the group at Wuhan University of Technology in May 2017 as a post-doc to study optoelectronic devices.



Dr. Dan Liu studied soft condensed matter physics in the University of Surrey since Oct. 2006, and was awarded a PhD in Jun. 2010. From Nov. 2010 to Aug. 2012, she was a post-doc research associate in the school of physics and astronomy, University of Leeds, working on lipid membrane. In 2013, Dan was awarded the "ChuTian" Scholar of Hubei province (China), and was appointed associate professor in the school of materials science & engineering at Wuhan University of Technology, China. Her research interests include soft matter physics and polymer materials.



Dr. Ahmed Iraqi obtained his BSc from the University of Fes (Morocco) in 1984. This was followed by an MSc in Chemistry from University Paul Sabatier in Toulouse in 1985 and a PhD from the same institution in 1988. Until 1996 he was a Postdoctoral Research Associate at the University of St Andrews, when he became a Lecturer at Lancaster University. In 2000 he was appointed Lecturer at the University of Sheffield, where he was promoted to Senior Lecturer in 2009 and Reader in 2013.



Prof. Tao Wang received a B.S. in Polymer Materials (2002) and an M.S. in Materials Science (2005). He obtained his Ph.D. in Physics from the University of Surrey (UK) in Feb. 2009. He then took a post-doc position in the same group until Oct. 2009 when he moved to the University of Sheffield (UK), where he worked with Prof. Richard Jones, FRS and Prof. David Lidzey on organic solar cells. He was awarded funding from “Recruitment Program of Global Experts” of China in 2013 and was appointed professor in Wuhan University of Technology (China). His research interests are optoelectronic devices, polymer physics and polymer materials.